Aftershocks Study of the 26 December 2003 Bam Earthquake

M. Tatar [1], D. Hatzfeld [2], A.S. Moradi [1], A. Paul [2], A.M. Farahbod [1], and M. Mokhtari [1]

1. Seismology Research Centre, International Institute of Earthquake Engineering and Seismology (IIEES), Tehran, Iran, email: mtatar@iiees.ac.ir
2. Laboratoire de Géophysique Interne et Tectonophysique, Grenoble, France

ABSTRACT: *From 29 December to 30 January, a dense seismological network of 20 stations surrounding the epicentral area of the 26 December 2003 Bam earthquake was installed to study the seismic activity that took place after the main shock. The aftershock distribution is consistent with a 30 km north-south striking fault. The focal depths distribution shows a nearly vertical alignment of aftershocks located between 6 to 20 km depth. The focal mechanism solutions indicate right lateral strike slip faulting on N-S trending fault, parallel to the Bam fault trace. However, there is a small offset of about 5km westward between the Bam fault trace and the aftershocks distribution.*

Keywords: Bam; Aftershocks; Strike slip fault; Focal mechanism; Local seismological network

1. Introduction

The active deformation of Iran is the result of Arabia-Eurasia convergence [1, 2], which is mainly accommodated by distributed deformation in the Zagros [13, 14], distributed faulting in the Alborz and Kopeh-Dagh mountain belts [18], and *N-S* right lateral shear between central Iran and Afghanistan. The major N-S right lateral fault systems east of Iran are the result of this shearing [17]. The overall convergence of the two Arabian and Eurasian plates is estimated to be about 30*mm/yr* at 50°*E* and 40*mm/yr* at 60°*E* [7, 9].

The present-day deformation of Iran deduced from *GPS* measurements [15] shows that about ~10*mm/yr* is accommodated in the Zagros. The rest is accommodated partly in the Alborz and Kopeh-Dagh (8+/-2*mm/yr*) and east of Iran on the Nayband-Gowk-Sabzevaran and Neh-Zahedan fault systems (8*mm/yr*). The eastern deformation of Iran has been the cause of the several recent large earthquakes up to magnitude of 7.0 that occurred during the last years [3]. The recent earthquake of December 26, 2003 (*Ms* = 6.5) near the small city of Bam, with around 26,500 human causalities, is one of the most destructive events that stroke this part of Iran. The seismogenic fault of this earthquake is a small fault between the two major strike slip fault systems of Nayband-Gowk-Sabzevaran and Neh-Zahedan on the west and east sides of the Dasht-e-Lut, see Figure (1).

The Bam earthquake occurred in a region where seismic activity is very low based on instrumental and historical catalogues for the last 2000 years, see Figure (2). As the figure shows, most of the historical and instrumental earthquakes located northwestern of Bam are related to activity on the Nayband, Gowk and Shahdad faults, and southwest of this city to the Jiroft active region. The 1854 Khorjand earthquake with an estimated intensity of *VIII*, the 1864 Chatrood historical event with a magnitude of *Ms*~6, and the 1897 Kerman-Chatrood earthquake with *Ms*~5.5 are the most important historical events that are located *NW* of Bam. As the largest instrumental earthquakes, which have occurred *NW* of the epicentral area of the Bam earthquake we can refer to the 11 June 1981 Golbaf earthquake (*Mw* = 6.6) and 28 July 1981 Sirch earthquake (*Mw* = 7.1). These events are associated with the activity of the Gowk fault. The most recent earthquake on this fault is the 14 March 1998 Fandoqa earthquake of magnitude *Mw* = 6.6 [3, 5, 6].

With the exception of the destructive earthquake of 26 December 2003, there is not any historical and

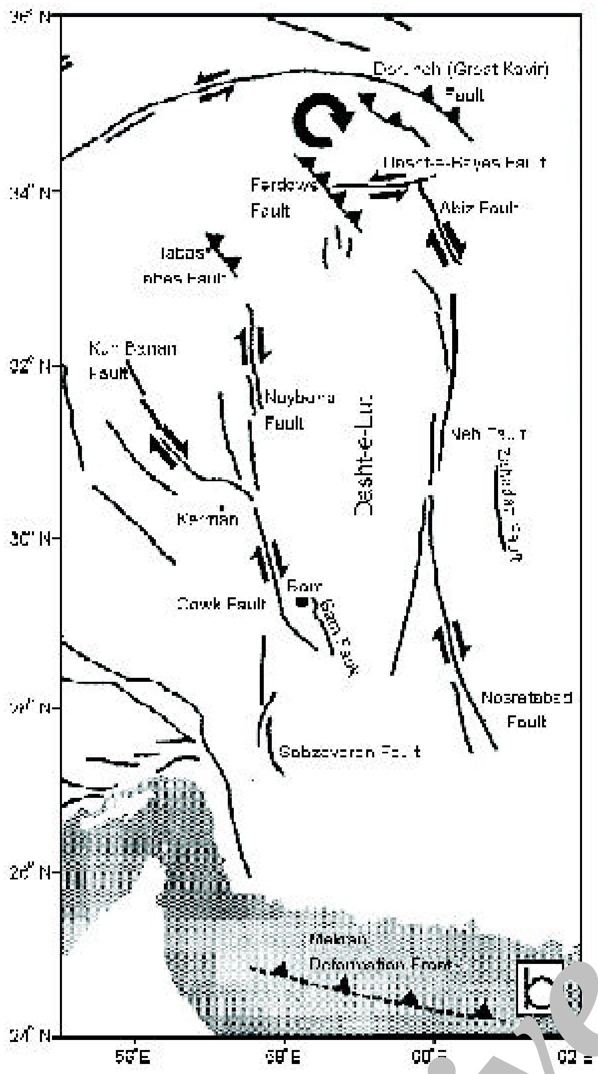

Figure 1. Major N-S trending, right lateral strike slip fault systems in eastern Iran [1].

instrumental earthquake recorded in the region surrounding Bam at least for distances closer than 120*km*.

In order to study aftershocks seismicity of the Bam earthquake, an array of 20 portable, 3-components stations was deployed around the epicentral area of the main shock on December 28, 2003, in an attempt to better understand the location, geometry and kinematics of the causative fault in the region. The experiment started 3 days after the main shock and lasted for a month. In this study, the results of the first week recording of aftershocks, from 29 December 2003 to 4 January 2004 are presented.

2. Recording and Analysis of Aftershocks

The 20-station temporary seismological network consisted of 10 short-period *CMG*-6*TD* seismometers connected to *CMG-DM*24 Guralp digitizers, and ten *CMG*-40*T* broadband seismometers, connected to MiniTitan recorders. The seismic instruments belonged to the Laboratoire de Géophysique Interne et Tectonophysique, University of Joseph Fourier, (France), and to the International Institute of Earthquake Engineering and Seismology (Iran). All stations were programmed to record in continuous mode. The signals from the short-period *CMG*-6*TD* were sampled at 100*Hz*, whereas a sampling rate of 62.5*Hz* was used for *CMG*-40*T* broadband seismometers. The stations were located around the epicenter of the main shock reported by *NEIC*, a few hours after the Bam earthquake, see Figure (2). More than 4000 events were recorded during the one-month duration of the experiment. The primary results of analyzing more than 500 aftershocks, recorded during the first week after the main shock, will be addressed in this paper.

More than 450 events recorded by at least 4 stations were selected. First, using *HYPO*71 [11], all the aftershocks (of magnitude ranging from 0.5 to 4.1) were located. Only 250 earthquakes were kept for which at least two *S* arrival times could be read. With a subset of 187 events, having a root mean square travel times residual (*RMS*) smaller than 0.2*s*, horizontal (*ERH*) and vertical (*ERZ*) uncertainties smaller than 2*km*, and an azimuthal gap smaller than 180°, a mean *Vp/Vs* ratio of 1.75+/-0.01 averaging *Ts-Tp/Tp-T*0 was computed. Then, the velocity structure of the crust assuming layers of variable thickness and of variable velocity was investigated. A one-dimensional velocity model obtained, see Figure (3) by inversion of the arrival times using the program *VELEST* [10] that relocates the earthquakes and simultaneously inverts for the velocity structure. The convergence of the inversion for 50 different starting models that are randomly distributed was checked, see Figure (3).

The simplest velocity structure obtained for the Bam region that fits our data consists of an upper layer 9*km* thick with a velocity of 5.7 *km/sec* overlying an half space of 6.4*km/sec*. The convergence of the obtained results in using several random starting models were tested. The resulting velocity model and station residuals were used in the Hypo71 locating program to relocate selected aftershock.

Lower-hemisphere fault plane solutions of single events were determined from first-motion data. The aftershocks with a minimum of 12 *P*-wave polarities were selected for the focal mechanism determination. The quality of the polarity reading, the type of wave

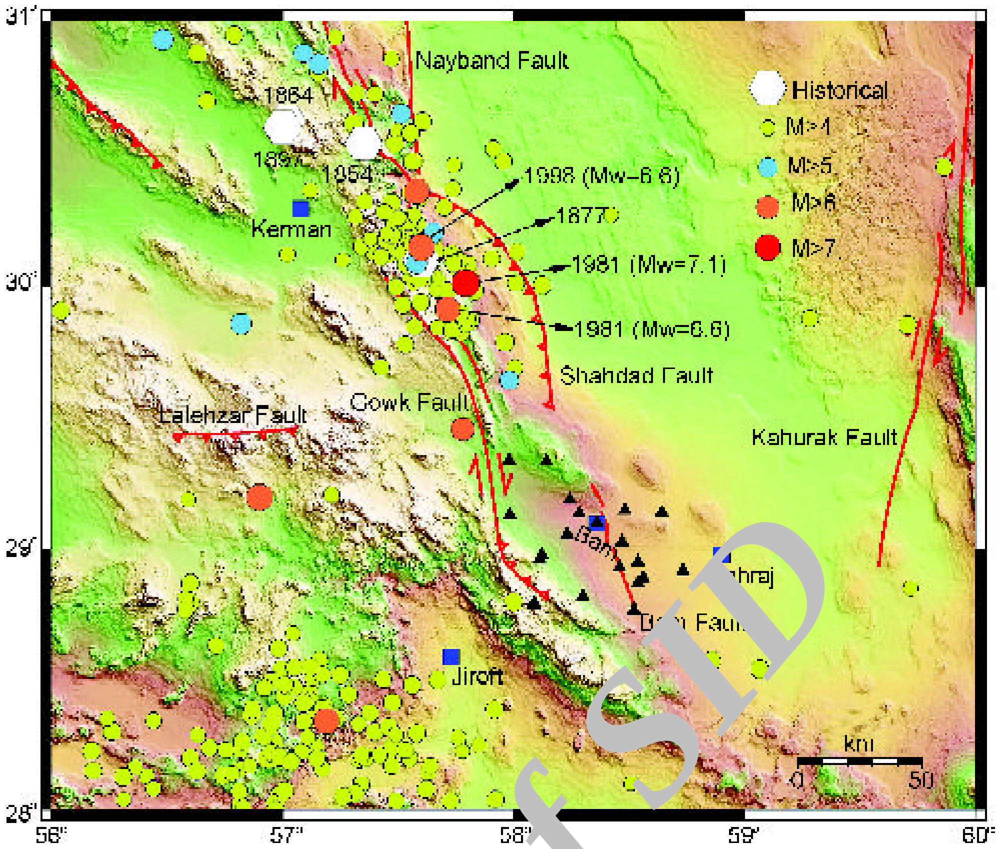

Figure 2. Seismicity map of historical and instrumental earthquakes in the regions surrounding the epicentral area of the Bam earthquake. Triangles indicate the location of temporary seismic stations.

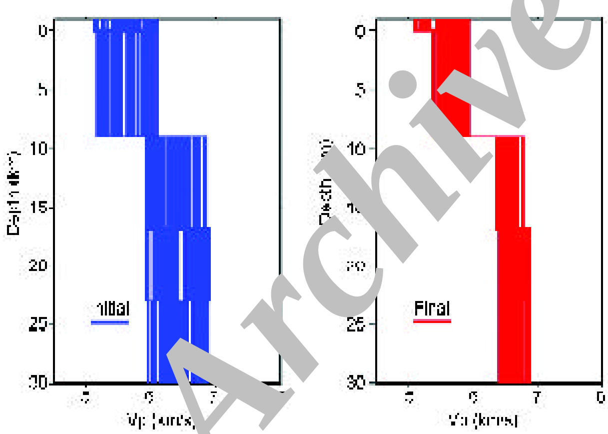

Figure 3. Velocity structure obtained for the shallow crust by inversion of the travel times of selected aftershocks recorded on the temporary seismological network. 50 random initial models (left) have been converged to a simple model consist of two layers (right).

(direct or refracted), and the azimuthal coverage on the focal sphere were taken into consideration in order to distribute the solutions into three categories depending on their reliability. In category A the mechanisms were used whose 3 quadrants are sampled and for which the two planes are constrained within 20°. In category *B*, only one plane was well constrained, but the orientation of the *P* and *T* axes were determined within 20°. In category *C*, none of the planes were constrained within 20°, and these solutions were used only to give an indication of the type of faulting.

Local magnitude (*M*l) was computed for more than 400 events, which indicate the aftershocks magnitude range between 0.5 and 4.0. Maximum pick-to-pick amplitudes was measured [8], after doing instrument correction and simulation of standardized instrument.

2. Aftershocks Distribution and Focal Mechanism

Among the 250-recorded aftershocks until January 4, 187 reliably located events (*ERH* and *ERZ*<2*km*, *RMS* < 0.2*sec*, *N*>12 stations) were selected that show a narrow *NS* trending aftershock zone, see Figure (4). This aftershock zone is centered on 29.10°*N* latitude and 58.37°*E* longitude. It is located right beneath the Bam city, which can explain the high level of destruction. The aftershock distribution defines a *N-S* trending zone extending from south to about 30*km* north of Bam roughly 7*km* wide.

The density of seismological stations ensures a

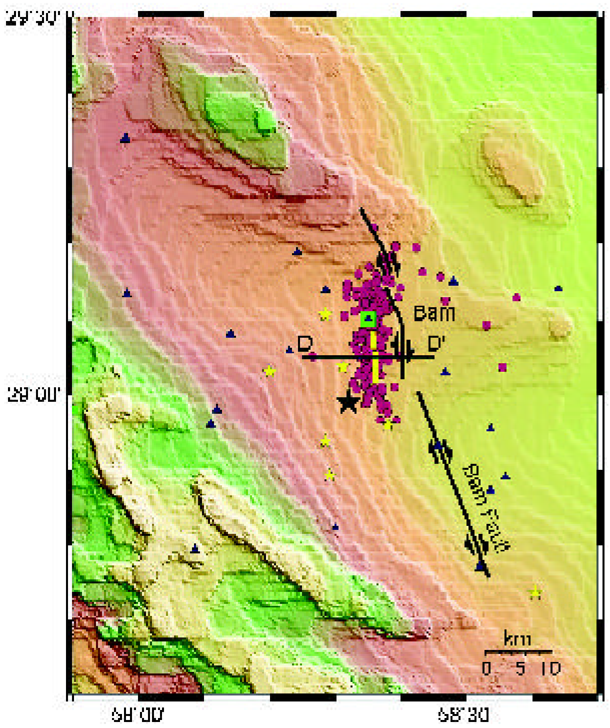

Figure 4. Seismicity map of the selected aftershocks recorded at more than 12 stations, with rms errors in time < 0.2s and in location < 2 km. The triangles are the seismological stations. The black star is the main shock and the yellow stars are the EHB teleseismically relocated main aftershocks (Engdahl, personal communication). The Bam fault is plotted in black and the seismic cracks in yellow.

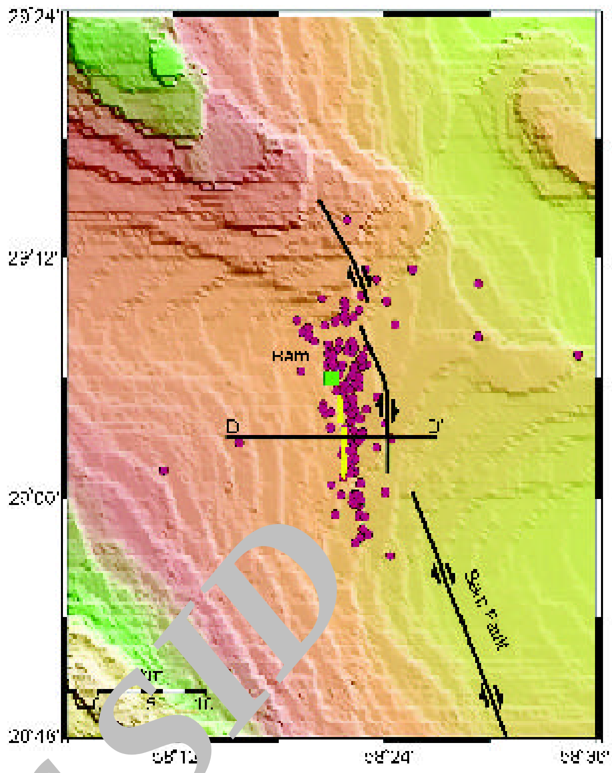

Figure 5. Seismicity map of the relocated aftershocks using the double difference method [15]. The distribution of relocated events shows a slightly more accurate picture of the seismogenic fault than the initial distribution.

much more accurate location than teleseismically located earthquakes. There is a systematic shift of ~10*km* to the *NE* relative to the *EHB* teleseismically relocated events, see Figure (4) by Engdahl (personal communication).

In order to refine the interpretation, the 180 earthquakes previously located with an uncertainty better than 2*km* both in epicenter and depth for events pairs with a minimum of 12 links were located, using the double difference method [16], see Figure (5). If the hypocentral location between events is small compared to the distance to the stations, the errors in the ray path are minimized. This method is particularly useful to map clusters of earthquakes and infer possible active faults. As Figure (5) shows, the seismicity is slightly better defined after relocating by the HypoDD technique. It confirms that the active fault was trending *NS* and dipping vertically.

The *E-W* cross section striking perpendicular to the distribution of aftershocks, see Figure (6) reveals that most of the seismicity is located between 6 and 20*km* of depth and therefore is likely to be located in the upper part of the crust. The distribution of focal depths based on the located (Hypo71) and relocated (HypoDD) selected aftershocks shows a fault plane dipping vertically.

A dense seismological network above the earthquakes provides a more complete coverage of the focal sphere than the teleseismic recording. Fault plane solutions for 40 aftershocks were computed, see Table (1). Most of the focal mechanisms within the aftershocks correspond to *NS* trending, right lateral strike slip faulting, in agreement with the seismicity and the mechanism of the main shock computed by *NEIC* and *HRDV*, see Figure (7) and Appendix (I). The trend of the *NS* trending fault planes is slightly (15°) rotated counterclockwise, which is consistent only with the rotation of northern termination of the Bam fault.

4. Discussion and Conclusion

A strong earthquake of magnitude (Mw = 6.5) devastated the city of Bam in the southeast of Iran. This earthquake occurred due to the rupturing of a fault, which is located within two major north-south, strike slip fault systems.

The distribution of aftershocks on map as well as

Table 1. Parameters of determined focal mechanisms.

Nb	Date	Time	Lat	Lon	Depth	Mag	Az1	Pl1	de1	Az2	Pl2	de2	Azp	dep	Azt	det	Im	Q
98	123103	11:33	29.07	58.35	13.53	1.4	55	80	-5.7	146	84.3	-170	10.8	11.1	280	3	-1	C
99	123103	11:44	29.06	58.35	10.00	2.4	95	80	-26.7	190	63.7	-169	-49.6	25.9	145	11	-1	D
100	123103	11:50	29.05	58.34	16.23	1.7	95	80	-26.7	190	63.7	-169	-49.6	25.9	145	11	-1	B
111	123103	14:57	29.07	58.35	14.97	1.6	55	80	-26.7	150	63.7	-169	9.6	25.9	105	11	-1	B
114	123103	15:36	29.00	58.37	10.00	2.5	80	80	-26.7	175	63.7	-169	34.6	25.9	130	11	-1	B
115	123103	15:43	29.07	58.35	13.75	1.3	60	70	-27.3	160	64.5	-158	18.6	33.1	111	3.6	-1	A
116	123103	15:52	29.03	58.35	12.80	1.7	130	80	-153	35	63.7	-11.2	355	25.9	260	11	-1	D
121	123103	18:45	29.02	58.36	11.05	2.1	65	80	26.7	160	63.7	169	19.6	25.9	115	11	1	A
122	123103	18:48	29.06	58.36	11.54	3	60	70	-14.3	155	76.5	-159	18.6	24	287	4.4	-1	A
128	123103	21:16	29.08	58.36	14.74	1.6	60	70	-14.2	155	76.5	-159	18.6	24	287	4.4	-1	B
130	123103	22:06	29.07	58.36	10.00	1.5	110	80	26.7	15	63.7	169	[illegible]	11	335	25.9	1	C
139	10104	2:39	29.01	58.36	11.51	1.4	140	80	26.7	45	[illegible]	[illegible]	[illegible]	11	5.4	25.9	1	B
143	10104	4:05	29.10	58.31	16.53	1.7	70	80	-26.7	165	[illegible]	[illegible]	24.6	25.9	120	11	-1	B
157	10104	10:06	29.09	58.37	16.38	1.6	240	80	-5.7	331	[illegible]	[illegible]	196	11.1	105	3	-1	B
158	10104	10:08	29.02	58.37	14.43	1.3	70	80	-153	[illegible]	[illegible]	-11.2	295	25.9	200	11	-1	B
160	10104	10:17	29.12	58.38	14.39	1.4	280	[illegible]	-26.7	[illegible]	[illegible]	-169	235	25.9	330	11	-1	B
162	10104	10:44	29.04	58.36	12.31	3.2	90	80	[illegible]	185	63.7	-169	-44.6	25.9	140	11	-1	C
164	10104	11:10	29.15	58.36	12.27	1.8	250	[illegible]	[illegible]	345	76.5	-159	209	24	117	4.4	-1	C
171	10104	13:43	29.04	58.37	13.23	3.4	100	[illegible]	-26.7	195	63.7	-169	54.6	25.9	150	11	-1	A
177	10104	16:09	29.07	58.34	16.50	1.9	240	80	-26.7	335	63.7	-169	195	25.9	290	11	-1	B
178	10104	16:52	29.05	58.37	14.50	1.5	65	80	5.7	334	84.3	170	19.8	3	289	11.1	1	A
181	10104	17:46	29.09	58.36	[illegible]	[illegible]	220	80	-26.7	315	63.7	-169	175	25.9	270	11	-1	B
190	10104	22:25	29.05	58.36	[illegible]	[illegible]	315	80	153	50	63.7	11.2	5	11	270	25.9	1	D
197	10204	2:52	29.13	[illegible]	[illegible]	1.6	155	50	90	335	40	90	245	5	65	85	1	A
201	10204	3:21	29.10	[illegible]	[illegible]	1.9	160	80	-153	65	63.7	-11.2	25.4	25.9	290	11	-1	A
202	10204	3:22	29.12	58.36	13.75	1.4	75	80	-21.9	169	68.4	-169	30.2	22.5	124	7.9	-1	A
204	10204	4:24	[illegible]	[illegible]	10.88	1.7	90	80	26.7	355	63.7	169	220	11	315	25.9	1	C
217	10204	[illegible]	[illegible]	58.36	16.76	1.6	70	80	-26.7	165	63.7	-169	24.6	25.9	120	11	-1	A
219	10204	[illegible]	[illegible]	58.36	13.75	1.4	85	80	-26.7	180	63.7	-169	39.6	25.9	135	11	-1	B
222	10204	[illegible]	29.05	58.37	12.40	1.8	85	80	-26.7	180	63.7	-169	39.6	25.9	135	11	-1	B
223	10204	12:28	29.09	58.35	15.91	1.5	150	80	-174	59	84.3	-10	14.2	11.1	105	3	-1	A
229	10204	16:19	29.13	58.37	14.85	1.9	265	80	-26.7	360	63.7	-169	220	25.9	315	11	-1	B
230	10204	16:56	29.04	58.36	10.72	1.4	60	80	-26.7	155	63.7	-169	14.6	25.9	110	11	-1	C
234	10204	17:55	29.10	58.35	11.58	1.6	235	80	5.7	144	84.3	170	190	3	99.2	11.1	1	B
236	10204	18:21	29.05	58.37	14.76	3.3	60	80	-26.7	155	63.7	-169	14.6	25.9	110	11	-1	A
238	10204	20:11	29.07	58.35	10.00	1.6	50	80	26.7	315	63.7	169	180	11	275	25.9	1	B
239	10204	20:28	29.08	58.34	16.39	1.4	55	75	-3.9	146	86.3	-165	11.4	13.2	280	7.9	-1	A
241	10204	20:38	29.04	58.36	11.92	1.5	80	80	-26.7	175	63.7	-169	34.6	25.9	130	11	-1	C

Lat, Lon, Depth are the coordinates of the aftershocks, Mag is the local magnitude, Az1, Pl1, de1, AZ2, Pl2, de2 are Azimuth, dip and slip of plane 1 and 2 respectively. Azp, dep, Azt, det are azimuth and dip of P- and T-axis respectively. Im is 1 for reverse and -1 for normal faulting respectively. A, B and C are a factor of quality of the fault plane solutions.

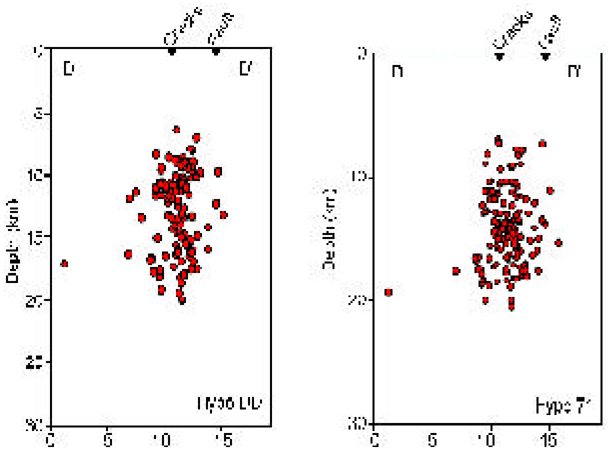

Figure 6. Cross-sections, trending EW of the selected aftershocks (Right) showing a fault plane dipping vertically. Focal depth of relocated events using double difference method (Left) defines the fault plane better than the initial hypocenters.

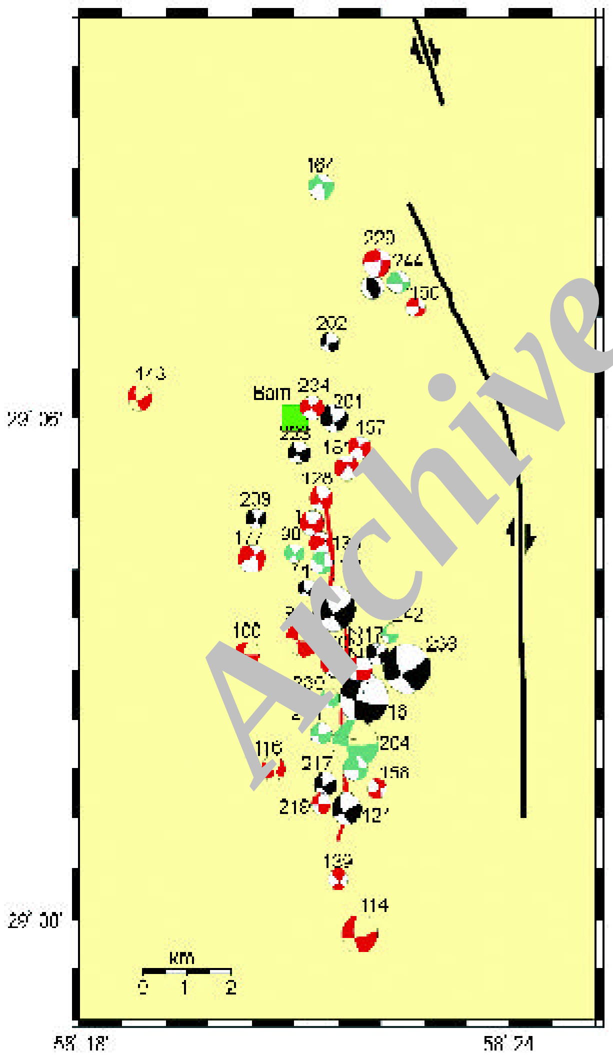

Figure 7. Map of the focal mechanisms for aftershock located better than 2km (horizontally and vertically), with a minimum of 12 polarities. The calculated focal mechanisms are divided to three groups based on their quality: A (Black), B (red) and C (green).

on cross-section indicates a *NS* striking seismogenic fault dipping vertically located precisely beneath the city of Bam. The focal depth distribution of relocated aftershocks does not support a westward dipping fault plane. The depth of the aftershocks are between 6 and 20*km*, and therefore deeper than the centroid depth of the main shocks computed by teleseismic body wave modeling [12].

The good consistency in direction for most of the *P*-axes, see Figure (8), specially in the southern part of the seismogenic fault, in addition of the *NS* trending, right lateral strike slip mechanisms, obtained for most of the aftershocks, south of Bam, does not support the existence of a secondary thrust fault as proposed by Talebian et al [12].

The counterclockwise rotation of *NS* trending nodal plane of some aftershocks, which is supported by clockwise rotation of *P*-axes north of the Bam, indicates a slight shortening component due to Arabia-Eurasia convergence north of Bam. The

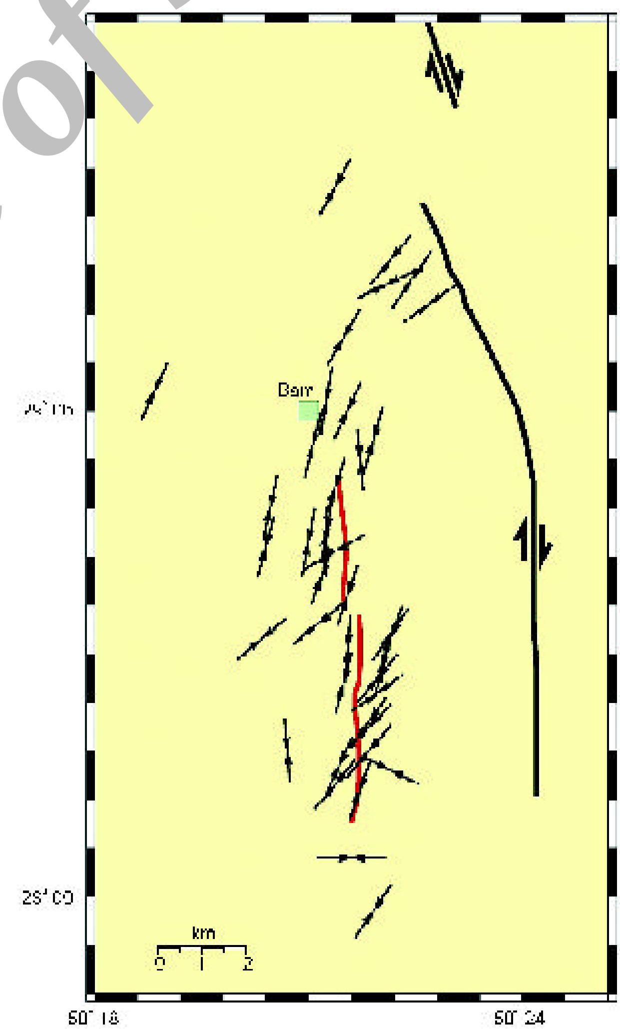

Figure 8. Horizontal projection of the P-axes associated with the focal mechanisms.

compressional component of a few fault plane solutions and the presence of at least one well constraint reverse focal mechanism, are another evidences on shortening effects of the northern part of the Bam seismogenic fault. However, it is not unusual to have reverse faulting at the termination of strike-slip faults.

One of the main questions raised after the Bam earthquake was related to the spatial extent of the rupture, since no surface rupture could be observed in the area. The spatial distribution and mechanism of the aftershocks reveal a seismogenic zone 30*km* long and ~7*km* wide, trending N-S, located right beneath Bam. A histogram of relocated aftershocks shows that the majority of earthquakes are located between ~6-20*km* of depth with a maximum number of events at 10-11 *km*, see Figure (9). No earthquakes located reliably at a depth greater than 20*km*, indicating that the seismicity is likely to be located in the upper part of the crystalline basement.

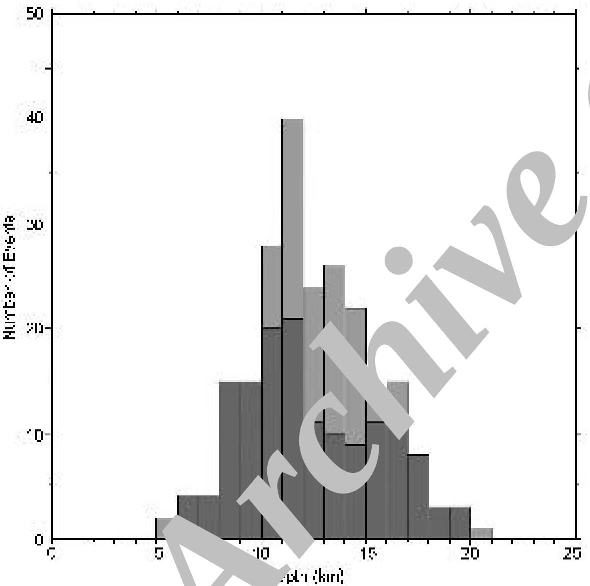

Figure 9. Depth distribution of aftershocks. Light purples for selected events. Dark is HypoDD relocated aftershocks. There is no seismic activity shallower than 5km.

Acknowledgment

This work was supported by *IIEES*. The authors are thankful to Dr. Mohsen Ghafory-Ashtiany for his help and support during the field experiment. The local seismological network was composed partially by French seismological *LITHOSCOPE* instruments. *DH* and *AP* thank French *INSU* for financial support. We would like to thank all observers and drivers who helped in the field. Some figures were generated by the Generic Mapping Tool (*GMT*) code developed by Wessel and Smith [19].

References

1. Berberian, M. (1981). “Active Faulting and Tectonics of Iran, in Zagros-Hindu-Kush-Himalaya Geodynamic Evolution”, Gupta, H.K., and Delany, F.M. (edts), *Am. Geophys. Union*, Geodyn. Ser., **3**, 33-69.

2. Berberian, M., King, G.C.P. (1981). “Towards a Paleogeography and Tectonic Evolution of Iran”, *Can. J. Earth Sci.*, **18**, 210-265.

3. Berberian M. and Qorashi, M. (1994). “Coseismic Fault-Related Folding During the South Golbaf Earthquake of November 20, 1989, in Southeast Iran”, *Geology* **22**, 531-534.

4. Berberian, M. and Yeats, R.S. (1999). “Pattern of Historical Earthquake Rupture in the Iranian Plateau”, *Bull. Seism. Soc. Am.*, **89**, 120-139.

5. Berberian, M., Jackson, J.A., Ghorashi, M., and Kadjar, M.H. (1984). “Field and Teleseismic Observation of the 1981 Golbaf-Sirch Earthquakes in SE Iran”, *Geophys. J. R. Astr. Soc.*, **77**, 809-838.

6. Berberian, M., Baker, C., Fielding, E., Jackson, J.A., Parsons, B.E., Priestley, K., Qorashi, M., Talebian, M., Walker, R., and Wright, T.J. (2001). “The March 14 1998 Fandoqa Earthquake (Mw = 6.5) in Kerman Province, SE Iran: Re-Rupture of the 1981 Sirch Earthquak e Fault, Triggering of Slip on Adjacent Thrusts, and the Active Tectonics of the Gowk Fault Zone”, *Geophys. J. Int.*, **146**, 371-398.

7. De Mets, C., Gordon, R.G., Argus, D.F., and Stein, S. (1994). “Effects of Recent Revisions to the Geomagnetic Reversal Time Scale on Estimates of Current Plate Motions”, *Geophys. Res. Lett.*, **21**, 2191-2194.

8. Hutton, L.K. and Boore, D. (1987). “The ML Sacle Southern California”, *Bull. Seis. Soc. Am.*, **77**, 2074-2094.

9. Jackson, J.A. (1992). “Partitioning of Strike-Slip and Convergent Motion between Eurasia and Arabia in Eastern Turkey and the Caucuses”, *Journal Geophys. Research*, **97**, 12471-12479.

10. Kissling, E. (1988). “Geotomography with Local Earthquake Data”, *Rev. of Geophys.*, **26**, 659-698.

11. Lee, W.H.K. and Lahr, J.C. (1972). HYPO71 (Revised), A Computer Program for Determining Hypocenters, Magnitude and First Motion Pattern of Local Earthquakes, *U.S. Geol. Surv. Open File Rep.*, 75-311.

12. Talebian, M., Fielding, E.J., Funning, G., Jackson, J., Nazari, H., Parson, B., Priestley, K., Qorashi, M., Rosen, P.A., Walker, R., and Wright, T.J. (2004). “The 2003 Bam (Iran) Earthquake-Rupture of “Truly Blind” Fault”, *Submitted to Geophys. Res. Lett.*

13. Tatar, M., Hatzfeld, D., Martinod, J., Walpersdorf, A., Ghafori-Ashtiany, M., and Chéry, J. (2002). “The Present Day Deformation of the Central Zagros (Iran)”, *Geophys. Res. Lett.*, **29**, 33-1 to 33-4, doi:10.1029/2002GL015159.

14. Tatar, M., Hatzfeld, D., and Ghafory-Ashtiany, M., (2004). “Tectonics of the Central Zagros (Iran) Deduced from Microearthqauke Seismicity”, *Geophys. J. Int.*, **156**, 255-266.

15. Vernant, Ph., Nilfroushan, F., Hatzfeld, D., Abbassi, M., Vigney, C., Masson, F., Nankali, H., Martinod, J., Ashtinay, M., Bayer, R., Tavakoli, F., Chery, J. (2004). “Contemporary Crustal Deformation and Plate Kinematics in Middle East Constrained by GPS Measurements in Iran and North Oman”, *Submitted to Geophys. J. Int.*

16. Waldhauser, F. and Ellsworth, W.L. (2000). “A Double Difference Earthquake Location Algorithm: Method and Application to the Northern Hayward Fault, California, *Bull. Seism. Soc. Am.*, **90**, 1353-1368.

17. Walker, R. and Jackson, J. (2002). “Offset and Evolution of the Gowk Fault, S.E. Iran: a Major Intra-Continental Strike Slip System”, *J. Structural Geology*, **24**, 1677-1693.

18. Walker, R., Jackson, J.A., and Baker, C. (2003). “Surface Expression of Thrust Faulting in Eastern Iran: Source Parameters and Surface Deformation of the 1978 Tabas and 1968 Ferdows Earthquake Sequences, *Geophys., J. Int.*, **152**, 749-765.

19. Wessel, P. and Smith, W.H.F. (2000). “The Generic Mapping Tools (GMT)”, University of Hawai’i.

Appendix I: Lower-hemisphere equal-area fault plane solutions for selected aftershocks. Compressional first motions are shown as solid circles, dilatation first motion as open circles. P-axes are shown as solid triangles and T-axes as open triangles.